

Inverse design of a 1D dielectric metasurface by topology optimization; fluctuations-trend analysis assisted by a diamond-square algorithm

K. EDEE^{1,*}, M. BEN RHOUMA^{1,2}, J.-A. FAN³, M. ANTEZZA², N. GIPPIUS⁴, E. WANG³, J.-P. PLUMEY¹, G. GRANET¹, AND B. GUIZAL²

¹Université Clermont Auvergne, Institut Pascal, BP 10448, F-63000 Clermont-Ferrand, France, CNRS, UMR 6602, Institut Pascal, F-63177 Aubière, France

²Laboratoire Charles Coulomb (L2C), UMR 5221 CNRS-Université de Montpellier, F-34095 Montpellier, France

³Department of Electrical Engineering, Stanford University, Stanford, California 94305, United States

⁴Skolkovo Institute of Science and Technology, Nobel Street 3, Moscow 143025, Russia

*Corresponding author: kofi.edee@uca.fr

Compiled September 23, 2020

We present a topology optimization (TO) method for a 1D dielectric metasurface, coupling the classical trend-fluctuations analysis (FTA) and the diamond-square- algorithm (DSA). In the classical FTA, a couple of device distributions termed Fluctuation or mother and Trends or father, with specific spectra is initially generated. The spectral properties of the trend function, allow to target efficiently the basin of optimal solutions. For optimizing a 1D metasurface to deflect a normally incident plane wave into a given deflecting angle, a cosine-like function has been identified to be an optimal father profile allowing to efficiently target a basin of local minima. However there is no efficient method to predict the father profile number of oscillations that effectively allows to avoid undesirable local optima. It would be natural to suggest a randomization of the variable which controls the number of oscillations of the father function. However, one of the main drawbacks of the randomness searching process is that, combined with a gradient method, the algorithm can target, undesirable local minima. The method proposed in this paper improves the possibility of the classical FTA to avoid the trapping of undesirable local optimal solutions. This is accomplished by extending the initial candidate family to higher quality offspring that are generated thanks to a diamond-square-algorithm (DSA). Doing so, ensures that the main features of the best trends are stored in the genes of all Offspring structures. © 2020 Optical Society of America

<http://dx.doi.org/10.1364/ao.XX.XXXXXX>

1. INTRODUCTION AND STATEMENT

Inverse design algorithms based on the topology optimization (TO) process have received significant attention in photonic device design [1–15]. The optimization process consists of three main parts: initialization, evaluation, and updating. During initialization, devices are set to have trivial or random dielectric distributions. These devices are then iteratively evaluated using the adjoint variables method, which yields gradients that specify how the device can improve a given figure of merit (FOM), and updated using gradient descent. TO has been successfully used to produce a broad range of freeform photonic devices operating in free space and on-chip, including metasurfaces, metagratings, wavelength routers, optical isolators, and photonic crystals [1–15]. As a gradient-based optimizer, TO is a local optimizer that is only capable of searching a limited region of the total design space, which is vast and non-convex. There are differ-

ent strategies allowing to more thoroughly search this space. Among them, a global optimum-inspired scenarios [16] and a well-defined initial condition strategy. In the second scenario, multiple optimizations are typically performed with differing initial dielectric distributions. An ensemble of locally optimized devices with a range of capabilities is produced, and the highest performing device is selected as the final device pattern. While this method works, it is computationally expensive and still limited to a set of local optimized devices, with limited search capabilities of the design space. However, an appropriate prediction of initial geometry features, can eliminate the drawbacks by efficiently targeting a basin of optimal local minimum and significantly reducing the computation time. The Fluctuation and Trends analysis (FTA), which combines the use of local gradients with an appropriate prediction of initial geometry features has been recently proposed [17] and it appears as a promising route avoiding a blind scan of the design

space. In this optimization scheme, two basic patterns with desired statistic properties are generated as initial devices geometry. The mother profile (or fluctuating function) holds the random fluctuations while the father provides the initial trend. The spectrum of the father distribution provides the main features of desired final binarized device. In the case of a 1D functional metasurface, a cosine-like function has been identified to be an optimal initial father profile yielding a desired final full-binarized structure. However there is no efficient method to predict the father profile number of oscillations that effectively allows to avoid undesirable local optima. Randomization of the variable controlling the father function shape is then required. But this stochastic process would be interesting only if it doesn't lead to a prohibitive cost in terms of computing time.

In this study, we explore a strategy termed Fluctuation and Trends Analysis-Diamond Square Algorithm (FTA-DSA), which combines the use of local gradients with an evolutionary-kind optimization. The proposed hybrid method is a promising route to expand TO to a global search of the design space. The augmentation of FTA with the DSA [18–20] allows to more systematically perform global optimization of photonic devices, by generating better initial candidates, while preserving the advantages introduced by the use of primary initial sinusoidal father profile function. The DSA has been firstly proposed by Fournier, Fussell and Carpenter [18] for the generation of two-dimensional landscapes or procedural texture with a very realistic-looking. It is commonly used in computer graphics software to model a surface or volume distribution of natural elements. Generally, the natural appearance *i.e.* the numerical representation of the randomness of these natural distribution is obtained by systematically performing interpolations of spatial values of some given nodes augmented with a random fractal noise function. This procedure provides a distribution of variables presenting both a random rendered and a self-similarity properties. The FTA assisted by the DSA works by taking multiple FTA-optimized devices, obtained after a very low number of iterations and systematically performing interpolations of the spatial characteristics of the best candidates of these devices to search within this design space region. We apply this algorithm to the optimization of one-dimensional metagratings, which consist of polysilicon nanoridges and that diffract an incident radiation into a given diffraction order. Metagratings are a good model system because they have a well-defined FOM, can be simulated accurately and with high speeds using solvers based on modal methods [21–30], and can be benchmarked with prior results.

2. METHODS

A. Basic concepts of the topology optimization by FTA

The FTA schematized in fig.1 is an iterative adjoint-based topology optimization method generally coupled with a gradient algorithm and used in the design of photonic devices. The algorithm starts with two initial continuous permittivity profiles, termed mother profile and father profile, possessing particular spectra that prevent the algorithm, as much as possible, being trapped in local minima. At iteration t , a *forward* and an *adjoint* (or reciprocal) computations (cf. fig.1) are performed yielding two kinds of electromagnetic fields, termed *direct field* and *adjoint field* respectively. These fields are then used to compute, (in a single run) at all points x_i of the design area, the gradient of the objective function $g^{(t)}(x_i)$. This computation, conceptually, consists in considering that fictitious currents are induced in the the structure when transits from a state denoted *old* to a state

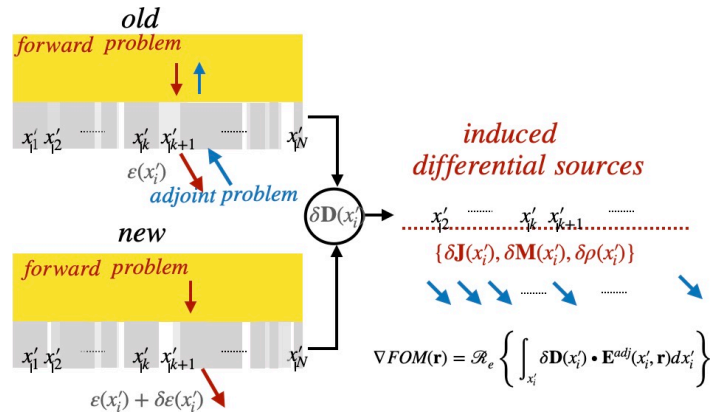


Fig. 1. Flowchart of the adjoint method used to compute the gradient of the figure of merit.

labelled *new*. This transition may be due to an evolution of the geometric or physical parameters of the system. The gradient is then used to modify the design variable values at each voxel of the design domain, in order to increase the FOM. The algorithm is performed iteratively, by pushing the continuous profile towards a discrete profile. This is accomplished through filtering (blurring) and projection (binarization) schemes in each step. A more detailed technical discussion on the computation of the gradient of the figure of merit applied here is provided in reference [17]. For those who are not familiar with the FTA concept, it may be useful to clarify the underlying motivations and intuitions guiding the choice of terms: mother profile and father profile. Father and Mother are terms commonly used in the theory of signal processing by the wavelet transform. Wavelets are defined by a wavelet function also called "mother" wavelet and a scaling function also called "father" wavelet. The wavelet function is a high band-pass filter (fluctuating function) while the scaling function filters the lowest level (scaling function). In the FTA, the couple of initial geometries have the same aspect and plays the same role as the father and mother wavelets used in signal processing. Besides, they handle the mean features of the final optimized structure: father geometry handles the global aspect (Trend or scale) while the mother profile holds the minimum size features. Now that this point is clarified, let's recall briefly the basic idea of the FTA scheme. During the first iteration, the mother profile becomes the old profile while the father profile is the new "trend". Only a forward simulation is performed on the father/new profile while a forward and adjoint computations (both computations are obtained with only one simulation) are performed on the mother/old profile. Hence a new profile is updated thanks to gradient based-like algorithm. The variable to be optimized, can undergo an ascending or descending increment as explained in reference [17]. At each iteration, and for each point of the design region, only the increment direction leading to the best result is kept. The ability of a gradient-based TO strategy, to yield satisfactory results, strongly depends on the initial conditions of the gradient-based algorithm. These initial geometries must be carefully selected to avoid undesirable local minima. In [17], while designing a 1D functional metasurface, a

cosine function

$$\rho_{trend}(x) = \frac{1}{2} \left[\cos \left(\frac{2\pi\eta}{d} x \right) + 1 \right], \quad (1)$$

has been identified to be an optimal father profile allowing to efficiently target a basin of local minima. This profile function depends on a parameter η which controls, both the maximum/ minimum feature sizes, and also the maximum number of nanorods of which the final binarized 1D metasurface is made up. The final optimized result may be, and in certain case, is, very sensitive to the variations of this parameter η . While a judicious choice of the father profile parameter η , systematically leads to a very rapid convergence towards a local minimum of the figure of merit, and this, independently of the mother function, a non judicious choice of η may drive the algorithm towards basins of undesired solutions. The instability introduced by the very high sensitivity of the FTA algorithm to the parameter η strongly penalizes the method. A trivial solution allowing to face this drawback, consists in randomly sweeping η -values on a given interval. However this randomized process can have a prohibitive cost in terms of computation time. The question is how to generate better initial candidates, preserving the advantages introduced by the use of the initial sinusoidal father profile function. The underlying idea of the solution we suggest is based on the use of the DSA in order to generate, from a set of initial best geometries, a basin of fittest individuals. In the next section, the basic sketch of the DSA is introduced.

B. The fluctuations-trend analysis (FTA) assisted by the diamond-square algorithm (DSA): FTA-DSA

For the optimization problem under consideration: designing a 1D metagrating capable of deflecting an incident wave to a given direction, we use the FTA to find an optimal permittivity function $\epsilon(x)$. In practice, the FTA is performed iteratively using a gradient-like method making it very sensitive to the initial conditions; which poses a problem of robustness. A trivial solution to this drawback, consists in randomly checking many initial profiles but, as is highlighted previously, this random process can have a prohibitive cost in terms of computation time.

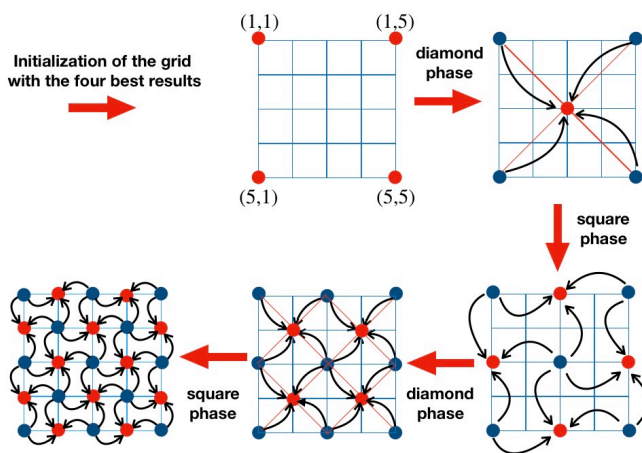


Fig. 2. Flowchart of the DSA performed on a 5×5 2D grid. Here n is set to $n = 3$, which means, that, after the initialization of the four corners of the grid, 2 cycles of diamond-square phases are implemented.

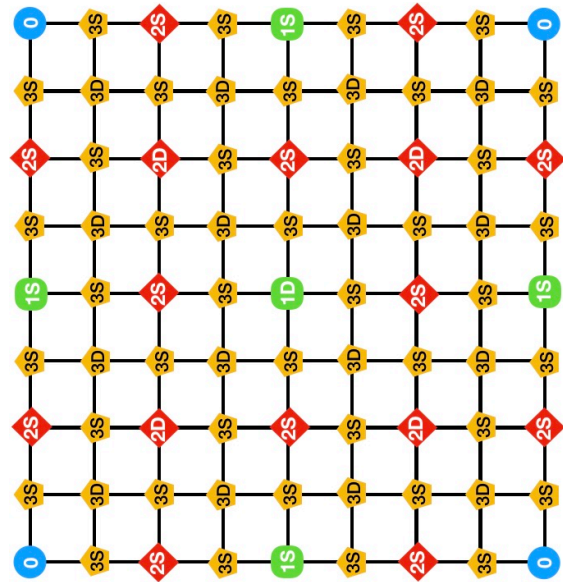


Fig. 3. Architecture of the 2D DSA grid obtained for $n = 4$ yielding a 9×9 2D grid. 3 cycles are performed. A node obtained at the end of the N th cycle is denoted Nd if it comes from a diamond phase and Ns if it is generated by a square phase.

Our idea is to perform the FTA with a small number of iterations using some initial profiles identified as the best candidates at a given iteration. At the beginning, we depart from a certain set of random candidates, run the FTA with a moderate number of iterations and select the four best among them. Then we use the DSA (the principle of which is given in the following) to generate an offspring of the latter and then run the FTA process over till a criterion (a given efficiency in a given diffraction direction) is satisfied. Thus the main role of the DSA, here, is to provide the FTA with a set of new generations with a sufficient variety yet holding the main characteristics of the four initial parents. For the readers not familiar with the DSA, we now provide the basic principles of this algorithm as applied in our problem. The diamond-square algorithm, firstly proposed by Fournier, Fussell and Carpenter [18], is a method originally devised to generate two-dimensional landscapes for computer graphics. The algorithm starts with the generation of a 2D grid of size $(2^{n-1} + 1) \times (2^{n-1} + 1)$, $n \neq 1$. At the beginning, the four corners of the 2D grid are initialized. In the optimization problem under consideration, we are interested in designing a permittivity function $\epsilon(x)$ of a metagrating, at some points x of the design area. Therefore the corners will be initialized by the four best candidates stemming from the first few FTA iterations.

After the initialization, two phases, namely *diamond phase* and *square phase*, are progressively and alternately performed until all values of the all nodes of the 2D grid have been set. The couple (diamond, square) determines a cycle of the DSA. For a given

value of the integer n , $n - 1$ cycles labelled p , ($p \in \mathbf{N} \cap [2, n]$) are performed to set all nodes of the 2D grid. In this paper n will also denote the order of the DSA. In the p^{th} cycle, one considers all $2^{p-1} \times 2^{p-1}$, ($p \in \mathbf{N} \cap [2, n]$), sub-squares. To the center of each of them (I, J) , we associate the average of $\varepsilon(x)$ over the corners :

$$\varepsilon^{(I,J)}(x) = \frac{1}{4} \sum_{i,j} \varepsilon^{(i,j)}(x) + \left(\frac{u}{2u}\right)^p (2r - 1) \quad (2)$$

where $u \in [0, 1]$ is a constant and r a random number in the range $[0, 1]$. The sum is performed on the value of the functions at the four closest nodes.

This phase is termed diamond because, drawing lines from the initial corners to the generated midpoint, leads to a diamond pattern. In the square phase, one considers all diamond-kind patterns made of the middle points computed in the previous diamond phase and the four previous square corners. The middle point of this diamond kind pattern is then computed as the average of these four nodes. The name square phase comes from the fact that by drawing lines from the corners to the midpoint one creates a square pattern. An illustration is given in fig. 2 where n is set to 3, which leads to a 5×5 2D grid. After the initialization of the four corners of the grid, two rounds of diamond-square steps are implemented. We present in fig. 3 the architecture of a 2D grid obtained from a higher order of DSA. In this figure, $n = 4$ yielding a 9×9 2D grid with 81 nodes. In order to facilitate the reading of the grid and for the sake of convenience, we adopt the following notation: a node obtained at the end of the N^{th} cycle is denoted ND if it comes from a diamond phase and NS if it is generated by a square phase. These nodes can also be identified by their coordinates (i, j) in the rectangular mesh.

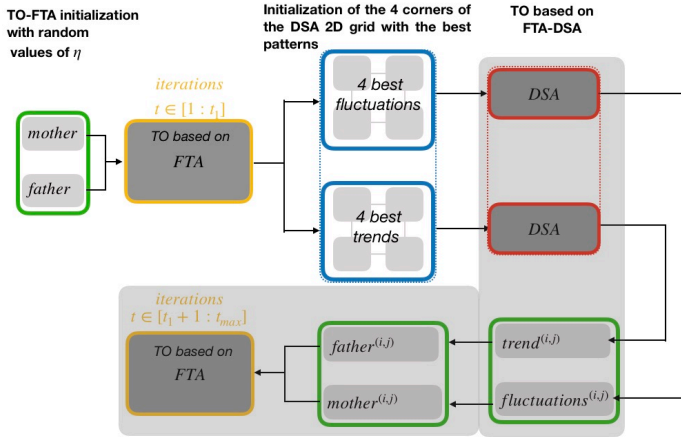


Fig. 4. Flowchart of the topology optimization based on FTA-DSA.

Equipped with these coupled algorithms, we are now ready to handle our design problem which is done in the next section.

3. RESULTS

We apply the proposed algorithm to the inverse design of 1D metagratings earlier studied in [11, 16], that deflect a normally-incident TM-polarized plane wave, with wavelength λ onto a particular transmitted angle θ_d . The optimized device consists of Si-nanorods with refractive index $\nu^{(2)} = 3.6082$, deposited

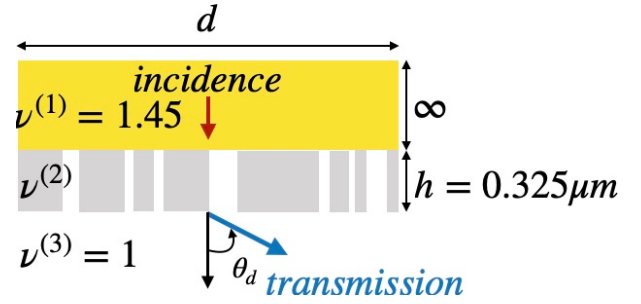


Fig. 5. 1D metagrating Geometry of a 1D metagrating deflecting a TM-polarized normal incident plane wave into θ_d angle

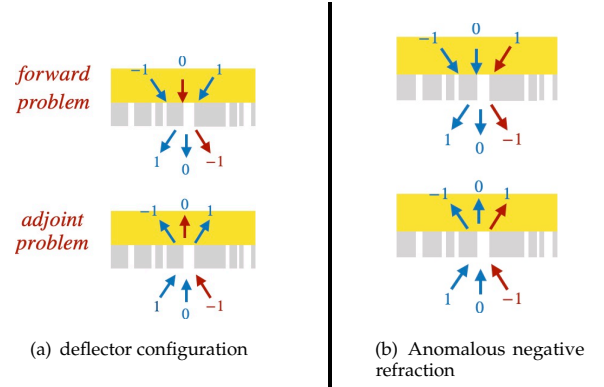


Fig. 6. Sketch of the direct and adjoint simulations used in the topology optimization of metagratings. Figures 6(a) and 6(b) present the direct and the adjoint computations methods for the deflector and anomalous refraction configurations respectively.

on a SiO_2 substrate ($\nu^{(1)} = 1.45$). The grating's height is set to $h = 0.325 \mu\text{m}$. See Fig. 5. In order to get the best devices allowing to initialize the DSA grid, we first generate a set of random values of the parameter η as follows:

$$\eta \in \{(\eta_{\max} - \eta_{\min})\text{rand}(1, N_\eta) + \eta_{\min}\}, \quad (3)$$

where N_η denotes the number of father profiles used as initial geometries in the first round of the FTA. The parameter N_η is set to $N_\eta = 10$, $\eta_{\max} = 5$ and $\eta_{\min} = 3.5$. For each father profile, the fluctuation or mother function is generated through a Druden-Veseky ocean bandlimited spectrum [31–36]. Table 1 presents results obtained on a 5×5 diamond-square 2D array. Two values of the incident field wavelength namely, $\lambda = 0.9 \mu\text{m}$ and $\lambda = 1.1 \mu\text{m}$ are investigated. The four initial parents are located at the four nodes $(1, 1)$, $(1, 5)$, $(5, 1)$ and $(5, 5)$ while all the other nodes correspond to the offspring results. As shown in this table satisfactorily high efficiencies are reached. Here five iterations are used in the first part of the FTA and 50 iterations are performed in the second round of the FTA. As expected, for the chosen incident wavelength, a large part of offspring leads to better fitness than parents. For $\lambda = 0.9 \mu\text{m}$, offspring of node $(2, 5)$ yields slightly better than the best father $\varepsilon^{(1,1)}$, while $\varepsilon^{(2,4)}$ is the best result for $\lambda = 1.1 \mu\text{m}$. $\varepsilon^{(i,j)}$ denotes the optimized permittivity profile associated with the nodes (i, j) of the DSA landscape.

Figures 7 present, some best optimized devices of the table 1. The initial father and mother profiles used in the second round of

$j \rightarrow$	1	2	3	4	5
	$\lambda = 0.9\mu\text{m}$				
$i \downarrow$					
1	0.9736	0.8925	0.9605	0.9695	0.9688
2	0.9624	0.9660	0.9616	0.9657	0.9742
3	0.8898	0.8930	0.8880	0.5886	0.6708
4	0.8963	0.8927	0.1979	0.6867	0.6210
5	0.8885	0.8890	0.3820	0.5845	0.9540
	$\lambda = 1.1\mu\text{m}$				
$i \downarrow$					
1	0.7806	0.7714	0.7775	0.7775	0.7492
2	0.7714	0.7714	0.7806	0.7825	0.7775
3	0.7714	0.7806	0.7678	0.7678	0.7621
4	0.7678	0.7714	0.7714	0.7678	0.7678
5	0.7652	0.7714	0.7678	0.7678	0.7621

Table 1. Panel of efficiencies of a 1D dielectric metasurface obtained by the FTA-DSA on a 5×5 2D grid for two values of wavelength: $\lambda = 0.9\mu\text{m}$ and $\lambda = 1.1\mu\text{m}$. The structure is optimized to deflect a normally TM polarized incident plane wave onto $\theta_d = 60^\circ$. Numerical parameters: $d = \sqrt{\epsilon_3}/\sin(\theta_d)$, $t_1 = 5$, $t_{max} = 55$, $\eta_{min} = 3.5$, $\eta_{max} = 5$, $N_\eta = 10$.

the TFA are also displayed in each case. Figure 7(a), shows the result obtained for $\lambda = 0.9\mu\text{m}$ from the best parent. While fig. 7(b) is related to initial elements obtained from inter-generational crosses. Recall that intergenerational cross breeding results in an average between permittivity functions of initial individuals. This explains the heckled-like specific shape of their trend and fluctuations profiles used in the second round of the TFA. As predicted, all these second-round couples of initial geometries hold similar features and yield final high performance auto-similar devices. The above observations are hold for a longer wavelength $\lambda = 1.1\mu\text{m}$. See figs. 7(c), and 7(d). From these results, it appears that that efficient devices operating with a couple ($\lambda = 0.9\mu\text{m}$, $\theta_d = 60^\circ$) are a 4-nanorods type while a 3-nanorods-kind is exhibited in the case of ($\lambda = 1.1\mu\text{m}$ at the same deflection angle $\theta_d = 60^\circ$). We compute, and plot in fig. 8 the real part of the magnetic field through the best optimized final device *i.e.* $\epsilon^{(2,5)}$. The deflection of the normally incident plane wave is clearly highlighted. In Figs. 9, we compare the efficiency histograms of optimized devices computed with the FTA and FTA-DSA, for $\lambda = 0.9\mu\text{m}$ (fig. 9(a)) and $\lambda = 1.1\mu\text{m}$ (fig. 9(b)) for $\lambda = 1.1\mu\text{m}$. As shown in these figures, 68% of the 25 realizations have efficiencies higher than 88%, indicating that the η -landscape is efficiently and broadly scanned for the chosen range namely $\eta \in [3.5, 5]$. These histograms also demonstrate clearly that adding DSA to the classical FTA provides systematically better results.

The strategy proposed so far consists in using the DSA only once during the optimization process. The FTA is first used, with a very low number of iterations in order to identify a quartet of best trends. Then the DNA of this quartet is disseminated through various offspring. Finally, a greater number of iterations of FTA is applied to each member of this new family. This scenario can be termed one-layer or unsupervised strategy. It seems obvious to consider a strategy based on a perpetual assessment of the initial conditions as the algorithm progresses. This strategy leads to a multi-layers or a supervised scheme. A supervised or multi-layers strategy, can be viewed as a concatenation of several slices/levels of FTA-DSA-FTA. In each layer, the FTA and DSA algorithms are performed alternatively, both

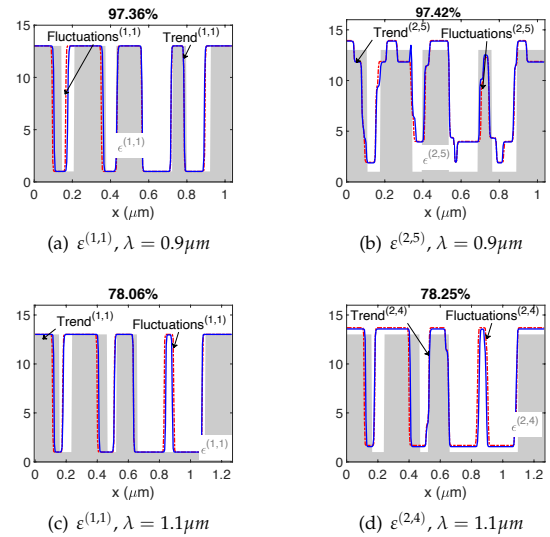


Fig. 7. Sketch of two final optimized devices for two wavelengths $\lambda = 0.9\mu\text{m}$ (figs. 7(a), 7(b)), and $\lambda = 1.1\mu\text{m}$ (figs. 7(c), 7(d)). The obtained optimized profile and the two initial geometries namely Trend and fluctuations profiles are displayed in each case. Numerical parameters: $\lambda = 0.9\mu\text{m}$, deflection angle $\theta_d = 60^\circ$, $t_1 = 5$, $N_{eta} = 5$, $\eta_{min} = 3.5$, $\eta_{max} = 5$, grating period $d = v_3\lambda/\sin(\theta_d)$.

with a very low number of iterations, about 5. First a FTA with very low numbers of iterations is performed, yielding a selection of the four best mother and father profiles at this iteration. These best profiles are then used for mapping the four corners of the next new DSA grid. A n order DSA is then applied leading to a $(2^{n-1} + 1) \times (2^{n-1} + 1)$ 2D initial individuals array. This new set of individuals are then used as initial geometries in a next FTA algorithm which is also performed with a low number of iterations. One can expect that this supervised strategy is an optimal scenario allowing to efficiently select, as earlier as possible, a class of unseen good optimal solutions. We apply the supervised strategy to the same example discussed earlier on table 1. Results are displayed on table 2. Recall that for this example, the structure is designed to deflect a TM normally incident plane wave onto 60° deflection angle for $\lambda = 0.9\mu\text{m}$ and $\lambda = 1.1\mu\text{m}$. One can remark that, the highest transmissions displayed on both tables are slightly different. For $\lambda = 0.9\mu\text{m}$, the highest efficiency from the multilevel FTA-DSA is 97.05% while this value reaches 97.42% in the case of classical or one-level FTA-DSA. For $\lambda = 1.1\mu\text{m}$, the high-performance structure provided by the classical FTA-DSA deflects 78.26% of the incident power while this deflected power reaches 79.37% when the multi-layers strategy is performed. As pointed out earlier, the maximum values of these two tables are hardly different. However, both results landscapes are fairly different. The multi-layers scheme exhibits a higher number of high-performing structures through the optimization process. For $\lambda = 0.9\mu\text{m}$ 40% of devices optimized thanks to the classical FTA-DSA, have a transmission efficiency greater than 90% while this ratio reaches 56% when the multi-layers scheme is performed. For $\lambda = 1.1\mu\text{m}$, 56% of optimized devices based on the classical FTA-DSA has a deflected power higher than 77% while the FTA-DSA supervised strategy yields 96%.

We perform, complementary analysis on devices operating with

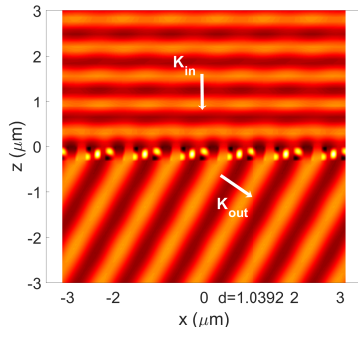


Fig. 8. TFA-DSA applied to design a 1D high-transmission deflection metagrating. Real part of the magnetic field. Illustration of the quality of the deflection phenomenon supported by one of the final highest-transmission devices ($\epsilon^{(2,5)}$). Numerical parameters: $\lambda = 0.9\mu\text{m}$, deflection angle $\theta_d = 60^\circ$, $t_1 = 5$, $N_{eta} = 10$, $\eta_{min} = 5$, $\eta_{max} = 3.5$, grating period $d = v_3\lambda/\sin(\theta_d)$.

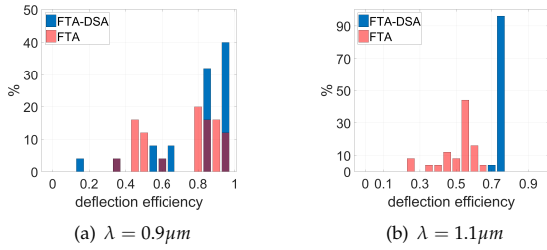


Fig. 9. Comparison of efficiencies histograms obtained with the FTA (ref color) and the FTA-DSA (blue) for $\lambda = 0.9\mu\text{m}$ (Fig. 9(a)) and $\lambda = 1.1\mu\text{m}$ (Fig. 9(b)). Numerical parameters: deflection angle $\theta_d = 60^\circ$, $t_1 = 5$, $N_{eta} = 10$, $\eta_{min} = 5$, $\eta_{max} = 3.5$, grating period $d = v_3\lambda/\sin(\theta_d)$.

a more large deflection angle. Generally, 1D metasurfaces designed to deflect an incident plane wave onto large deflection angles have bad performances. In this case, it is difficult to exhibit high-performance structures from a set of random initial conditions since the design space with a multitude and very close basins of local minima. Consequently, the gradient-based method faces a multitude of basins of local minima and a huge number of initial candidates is required before satisfactory solutions are reached. A way to generate initial candidates allowing to broadly and efficiently span the design space consists in increasing the DSA order n . Figure 10(a) shows the comparison between the histograms obtained with the FTA and FTA-DSA, of optimized devices for $\lambda = 0.9\mu\text{m}$ while the histograms corresponding to $\lambda = 1.1\mu\text{m}$ are reported in fig. 10(c). The highest-transmission device is also displayed on each figure. The DSA order is set to $n = 4$ yielding a 9×9 grid. The projection of optimized devices landscape on the DSA 2D array is presented in figure 10(b) and 10(d) for $\lambda = 0.9\mu\text{m}$ and $\lambda = 1.1\mu\text{m}$, respectively. It is worth noting, from all these results that the FTA-DSA scheme enforces the trend towards particular basins of local minima, leading to a partition of devices histogram and DSA 2D landscape, onto several narrow disjointed sub-bands and sub-sections respectively. Let's also highlight that, for the current deflection angle, namely $\theta = 80^\circ$, the results obtained from FTA-DSA still provide systematically better results than the FTA.

$j \rightarrow$	1	2	3	4	5
$i \downarrow$	$\lambda = 0.9\mu\text{m}$				
1	0.9427	0.9705	0.9705	0.9486	0.9669
2	0.9705	0.9705	0.3105	0.9658	0.3221
3	0.9666	0.9605	0.9605	0.3145	0.3021
4	0.9619	0.2999	0.3125	0.3021	0.2992
5	0.9568	0.2788	0.3218	0.3009	0.9669
$i \downarrow$	$\lambda = 1.1\mu\text{m}$				
1	0.7735	0.7923	0.7918	0.7937	0.7735
2	0.7787	0.7890	0.7982	0.7777	0.7937
3	0.7890	0.7890	0.7726	0.7876	0.7872
4	0.7809	0.7809	0.7876	0.7746	0.7872
5	0.7565	0.7934	0.7809	0.7872	0.7727

Table 2. Panel of efficiencies of a 1D dielectric metasurface obtained by a TO based on a 10 layers-supervised/multi-layers FTA-DSA-FTA. The algorithm is performed on a 5×5 2D grid for two values of wavelength: $\lambda = 0.9\mu\text{m}$ and $\lambda = 1.1\mu\text{m}$. The structure is optimized to deflect a normally TM polarized incident plane wave onto $\theta_d = 60^\circ$. Numerical parameters: $d = \sqrt{\epsilon_3}/\sin(\theta_d)$, $t_1 = 5$, $t_{max} = 55$, $\eta_{min} = 3.5$, $\eta_{max} = 5$, $N_\eta = 10$.

This fact indicates that the algorithm improves the possibility of the classical FTA to avoid the trapping of undesirable local optimal solutions.

Finally, in order to justify the generalization of the proposed approach, staying in the case of 1D functional dielectric metagrating optimization, we apply the concept to successfully realize a ultra-high-efficiency anomalous refraction with a 1D dielectric metagrating [12]. As highlighted by Snell et al. in [12], the realization of metagratings handling this physical phenomenon for arbitrary input (incident) and output angles remains a challenge. Here, we numerically show that the proposed optimization method allows to efficiently design ultra-high-efficiency anomalous refraction dielectric metagratings and can yield arbitrary input and output angles. We consider the same structure used in the previous study and it is designed to deflect $\theta_{in} = +36.67^\circ$ TM incident planewave to $\theta_{out} = -60^\circ$ output planewave at $\lambda = 0.9\mu\text{m}$ operating wavelength. The configuration of the study is displayed in fig. 6(b). Figure 11(a) shows the histogram of the devices optimized thanks to the FTA-DSA. FTA-DSA is performed on a 5×5 DSA grid. Nearly 50% of the optimized structures transmit more than 90% of the incident energy. The optimal structures are a 3-nanorods type with a deflected efficiency close to 95%. The quality of the deflection phenomenon supported by one of the final highest-transmission devices is illustrated in fig. 11(b) where we plot the real part of the magnetic field. The incident and deflected wavefronts are well-distinguished.

4. CONCLUSION

We design a functional 1D dielectric metasurface based on a topology optimization method. The proposed algorithm is based on the fluctuation and trends analysis which initially performs, randomly, a very large class of non-intuitive solutions in the design space. The trend is a simple shape deterministic oscillatory function while a set of optimal fluctuating initial geometries are generated through a random Gaussian process with suited bandlimited correlation function spectrum. A suited choice of

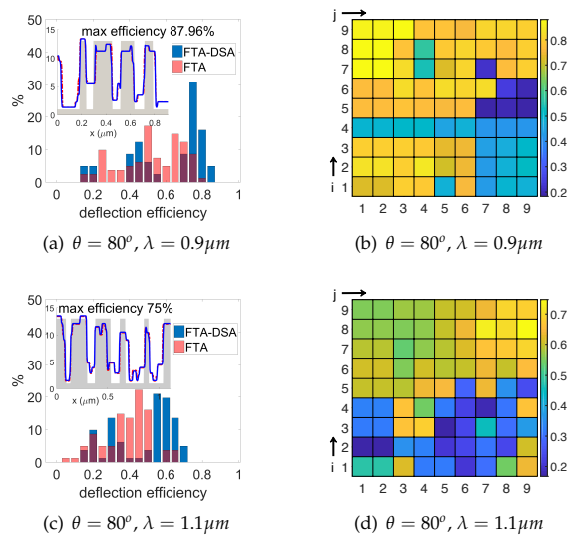


Fig. 10. TFA-DSA applied to design a 1D high-transmissive metasurface deflecting TM incident planewave onto $\theta_d = 80^\circ$. Figures 10(a) and 10(c) shows the histogram of optimized results for $\lambda = 0.9\mu\text{m}$ and $\lambda = 1.1\mu\text{m}$ respectively. The DSA order is set to $n = 4$ yielding a 9×9 grid. The projection of optimized devices landscape on the DSA 2D array is presented in figure 10(b) and 10(d) for $\lambda = 0.9\mu\text{m}$ and $\lambda = 1.1\mu\text{m}$, respectively.

the trend feature allows to efficiently target optimal solutions. Since, no method can efficiently predict the trend profile features, we suggest a randomization of the number of oscillation of the trend function. A randomness exploration process begins by tracking the best initial candidates through a low number of FTA-iterations. Using a diamond-square-algorithm (DSA), the best initial candidates family is extended to higher quality offspring that handle the DNA feedback. We successfully apply the method to design a 1D metagrating that deflects an incident TM polarized wave into several angles for different wavelengths. We showed that, the probability to reach a high-performance structure is highly increased, despite the full randomization of the initial profile mean features.

FUNDING INFORMATION

This work has been sponsored by the French government research program "Investissements d'Avenir" through the IDEX-ISITE initiative 16-IDEX-0001 (CAP 20-25)

DISCLOSURES

The authors declare no conflicts of interest.

REFERENCES

1. J. Lu and J. Vuckovic "Nanophotonic computational design," *Opt. Express* **21**, 13351-13367, (2013).
2. C. M. Lalau-Keraly, S. Bhargava, O. D. Miller and E. Yablonovitch, "Adjoint shape optimization applied to electromagnetic design," *Opt. Express* **21**, 21693-21701 (2013)
3. T. W. Hughes, M. Minkov, I. A. D. Williamson, and Shanhuai Fan, "Adjoint Method and Inverse Design for Nonlinear Nanophotonic Devices" *ACS Photonics* **2018**, **5**, 4781-4787, (2018).

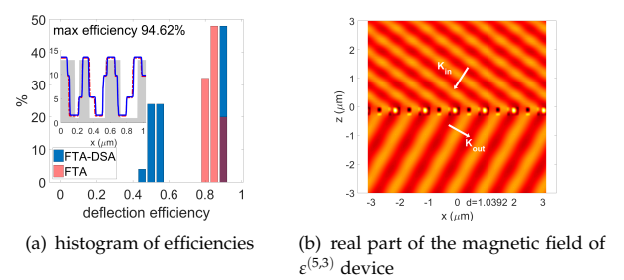


Fig. 11. Illustration of a negative refraction based on the FTA-DSA. The optimized 1D dielectric metagrating deflects an incident plane wave with incidence $\theta_{in} = +36.67^\circ$ into $\theta_{out} = -60^\circ$. Figure 11(a) shows the histogram of the optimized devices and one of the best structure. The father profile is draw in blue and the mother is in dash line red color. Fig. 11(b) shows the real part of the magnetic field in order to illustrate the quality of the deflection phenomenon supported by one of the final highest-transmission devices. Numerical parameters: $\lambda = 0.9\mu\text{m}$, grating period $d = v_3\lambda/\sin(\theta_d)$.

4. S. Molesky, et al. "Inverse design in nanophotonics," *Nat. Photonics* **12**, 659-670, (2018).
5. L. H. Frandsen, et al. "Broadband photonic crystal waveguide 60° bend obtained utilizing topology optimization," *Opt. Express* **12**, 5916-5921 (2004).
6. P. I. Borel, et al. "Topology optimization and fabrication of photonic crystal structures," *Opt. Express* **12**, 1996-2001 (2004).
7. A. Y. Piggot, et al. "Inverse design and demonstration of a compact and broadband on-chip wavelength demultiplexer," *Nat. Photonics* **9**, 374-377 (2015).
8. T. P. Xiao, et al. "Diffractive spectral-splitting optical element designed by adjoint-based electromagnetic optimization and fabricated by femtosecond 3D direct laser writing," *ACS Photonics* **3**, 886-894 (2016).
9. Lin, Z. et al. "Topology-optimized multilayered metaoptics," *Phys. Rev. Appl.* **9**, 044030 (2018).
10. D. Sell, J. Yang, S. Doshay, R. Yang, and J. A. Fan, "Large-angle, multifunctional metagratings based on freeform multimode geometries," *Nano Lett.* **17**, 3752-3757 (2017).
11. J. Yang J. A. Fan "Topology-optimized metasurfaces: impact of initial geometric layout," *Opt. Letters* **42**, 3161-3164 (2017).
12. D. Sell, J. Yang, E. W. Wang, T. Phan, S. Doshay, and J. A. Fan, "Ultra-High-Efficiency Anomalous Refraction with Dielectric Metasurfaces," *ACS Photonics* **5**, 2402-2407 (2018).
13. J. Yang, D. Sell, and J. A. Fan, "Freeform metagratings based on complex light scattering dynamics for extreme, high efficiency beam steering," *Ann. Phys.* **530**, 1700302 (2018).
14. T. Phan, D. Sell, E. W. Wang, S. Doshay, K. Edee, J. Yang, and J. A. Fan, "High-efficiency, large-area, topology-optimized metasurfaces," *Light. Sci. Appl.* **8**, 48 (2019).
15. E. W. Wang, D. Sell, T. Phan, and J. A. Fan, "Robust design of topology-optimized metasurfaces," *Opt. Mater. Express* **9**, 469-482 (2019).
16. J. Jiang, D. Sell, S. Hoyer, J. Hickey, J. Yang, and J. A. Fan, "Freeform diffractive metagrating design based on generative adversarial networks," *ACS Nano* **13**, 8872-8878 (2019).
17. K. Edee "Topology optimization of photonics devices: fluctuation-trend analysis concept; random initial conditions with Gaussian and Durden-Vesecy power density bandlimited spectra," *JOSAB* **37**, 2111-2120 (2020).
18. A. Fournier, D. Fussell, L. Carpenter, "Computer rendering of stochastic models," *Communications of the ACM.* **25** (6): 371-384, (1982).
19. Miller, S. P. Gavin. "The definition and rendering of terrain maps". *ACM SIGGRAPH Computer Graphics.* **20** (4): 39-48, (1986).
20. J. P. Lewis, "Generalized stochastic subdivision". *ACM Transactions on Graphics.* **6** (3): 167-190, (1987).

21. K. Knop "Rigorous diffraction theory for transmission phase gratings with deep rectangular grooves," *J. Opt. Soc. Am. A* **68**, 1206-1210 (1978)
22. G. Granet and B. Guizal "Efficient implementation of the coupled-wave method for metallic lamellar gratings in TM polarization," *J. Opt. Soc. Am. A* **13**, 1019-1023 (1996)
23. P. Lalanne and G. M. Morris "Highly improved convergence of the coupled-wave method for TM polarization," *J. Opt. Soc. Am. A* **13**, 779-784 (1996)
24. L. Li "Use of Fourier series in the analysis of discontinuous periodic structures," *J. Opt. Soc. Am. A* **13**, 1870-1876 (1996)
25. G. Granet, "Reformulation of the lamellar grating problem through the concept of adaptive spatial resolution," *J. Opt. Soc. Am. A* **16** 2510-2516 (1999).
26. K. Edee "Modal method based on subsectional Gegenbauer polynomial expansion for lamellar grating," *J. Opt. Soc. Am. A* **28** 9 , (2011)
27. K. Edee, I. Fenniche, G. Granet, B. Guizal "Modal method based on subsectional Gegenbauer polynomial expansion for lamellar gratings: Weithing function, convergence and stability," *PIER*, **133** 17-35, (2013)
28. K. Edee, B. Guizal "Modal method based on subsectional Gegenbauer polynomial expansion for nonperiodic structures: complex coordinates implementation," *J. Opt. Soc. Am. A* **30**, 4, 631-639 (2013)
29. Kofi Edee, J.-P. Plumey "Numerical scheme for the modal method based on subsectional Gegenbauer polynomial expansion: application to biperiodic binary grating," *J. Opt. Soc. Am.* **31**, 402-410 (2015)
30. Kofi Edee, J.-P. Plumey, B. Guizal "Unified Numerical Formalism of Modal Methods in Computational Electromagnetics and Latest Advances: Applications in Plasmonics" Elsevier, *Advances in Imaging and Electron Physics Vol. 197*, chapter 2 (2016)
31. G. R. Valenzuela, "Theories for interaction of electromagnetic and oceanic waves: a review," *Bound. Layer Meteorology*, **13**, 61-85 (1978).
32. L. B. Wetzel, "Sea clutter," *Radar Handbook*, Chap. **13** 2nd edition, M. Skolnik, ed., McGraw-Hill, Now York (1990).
33. J. R. Apel, "An improvement model of the ocean surface wave vector spectrum and its effects on radar backscatter," *J. Geophys. Res.*, **99**, 16269-16291 (1994).
34. S. L. Druden and J. F. Vesecky, "A physical cross-section model for a wind driven sea with swell," *IEEE J. Ocean. Eng.* **10**, 445-451 (1985).
35. S. H. Yueh, "Modeling of wind direction signal in polarimetric sea surface brightness temperatures," *IEEE Trans. Geosci. Remote Sens.*, **35**, 1400-1418 (1997).
36. S. H. Yueh, R. Kwok , F. K. Li, S. V. Nghiem , W. J. Wilson and J. A. Kong "Polarimetric passive remote sensing of ocean wind vectors," *Radio Sci.*, **29**, 799-814 (1994).
37. Clausnitzer, T.; Kampfe, T.; Kley, E. B.; et al. "Investigation of the polarization-dependent diffraction of deep dielectric rectangular transmission gratings illuminated in Littrow mounting," *Appl. Opt.* 2007, **46**, 819-826.
38. K. Hehl; J. Bischoff; U. Mohaupt ; et al. "High-efficiency dielectric reflection gratings: design, fabrication, and analysis," *Appl. Opt.* 1999, **38**, 6257-6271.